Monitoring disease progression in transgenic mouse models of Alzheimer's disease with proton magnetic resonance spectroscopy

Malgorzata Marjanska*†, Geoffrey L. Curran‡, Thomas M. Wengenack‡, Pierre-Gilles Henry*, Robin L. Bliss§, Joseph F. Poduslo‡, Clifford R. Jack, Jr.¶, Kâmil Uğurbil*, and Michael Garwood*§

*Center for Magnetic Resonance Research and Department of Radiology, and §Cancer Center, University of Minnesota, Minneapolis, MN 55455; and Departments of ‡Neurology, Neuroscience, Biochemistry/Molecular Biology, and ¶Radiology and Magnetic Resonance Research Laboratory, Mayo Clinic College of Medicine, Rochester, MN 55902

Communicated by Alexander Pines, University of California, Berkeley, CA, June 30, 2005 (received for review June 1, 2005)

Currently no definitive biomarker of Alzheimer's disease (AD) is available, and this impedes both clinical diagnosis in humans and drug discovery in transgenic animal models. Proton magnetic resonance spectroscopy (^{1}H MRS) provides a noninvasive way to investigate *in vivo* neurochemical abnormalities. Each observable metabolite can potentially provide information about unique *in vivo* pathological processes at the molecular or cellular level. In this study, the age-dependent ^{1}H MRS profile of transgenic AD mice was compared to that of wild-type mice. Twenty-seven APP-PS1 mice (which coexpress mutated human presenilin 1 and amyloid-β precursor protein) and 30 wild-type mice age 66–904 days were examined, some repeatedly. A reduction in the levels of *N*-acetylaspartate and glutamate, compared with total creatine levels, was found in APP-PS1 mice with advancing age. The most striking finding was a dramatic increase in the concentration of *myo*-inositol with age in APP-PS1 mice, which was not observed in wild-type mice. The age-dependent neurochemical changes observed in APP-PS1 mice agree with results obtained from *in vivo* human MRS studies. Among the different transgenic mouse models of AD that have been studied with ^{1}H MRS, APP-PS1 mice seem to best match the neurochemical profile exhibited in human AD. ^{1}H MRS could serve as a sensitive *in vivo* surrogate indicator of therapeutic efficacy in trials of agents designed to reduce neurotoxicity due to microglial activation. Because of its noninvasive and repeatable nature, MRS in transgenic models of AD could substantially accelerate drug discovery for this disease.

myo-inositol | taurine | drug discovery

Proton magnetic resonance spectroscopy (^{1}H MRS) provides a noninvasive way to investigate *in vivo* neurochemical abnormalities of many brain disorders. In particular, MRS is particularly well suited for the study of neurodegenerative disorders, because no biomarkers for such disorders currently exist. Each observable metabolite can potentially provide unique information about the degenerative process, because metabolite levels are sensitive to different *in vivo* pathological processes at the molecular or cellular level. For example, *N*-acetylaspartate (NAA) is believed to be a marker for neuronal number and health, glutamate (Glu) acts as an excitatory neurotransmitter, and *myo*-inositol (mIns) is thought to be a marker for osmotic stress or astrogliosis.

Alzheimer's disease (AD) is the most common cause of dementia in the elderly. The primary risk factor for AD is age. As the population of virtually all modern industrialized societies ages, AD is poised to become a leading public health problem. The vast majority of prevalent cases of AD are sporadic. The remaining few percent of familial cases are attributed to specific mutations. Three known classes of mutations are associated with familial AD. Although statistically uncommon, the genetic associations with familial AD have shed insight into the origins of the disease. It is believed by many in the field that AD is related to dysfunctional metabolism of β-amyloid protein in the brain of affected individuals. All known human mutations associated with familial AD alter production or clearance of β-amyloid protein.

The development of transgenic mouse models for AD enables controlled study of disease mechanisms and testing of therapeutics. There are three general types of AD mouse models. In the first model, mutated forms of human amyloid-β precursor protein (APP) are overexpressed in mice (1–4), which develop amyloid plaques predominantly in the neocortex and the hippocampus by 10 months of age. Accelerated amyloid deposition was achieved in the second mouse model in which mice coexpress mutated human presenilin 1 (5) and APP proteins (APP-PS1) (5, 6). The amyloid plaques start to appear at 3 months of age (6, 7). The third mouse model overexpresses mutant forms of human presenilin 2 (PS2) and human APP (PS2APP) (8). These mice develop a severe cerebral amyloidosis exclusively in the neoortex and the limbic cortex, including the hippocampus and amygdala as well as the thalamic and pontine nuclei at 8 months.

MRS analyses of single-transgenic APP (9) and double-transgenic PS2APP (10) mouse brains show altered neurochemical profiles. In a recent study, the neurochemical profiles of age-matched (19 $\pm$ 2 months of age) APP_{Tg2576} and wild-type littermates were compared (9). Based on the spectra obtained both *in vivo* and *in vitro* from a 36-μl voxel centered over the cingulate cortex and extended to include the sensorimotor cortex, it was concluded that the levels of NAA, Glu, and glutathione were lower, and the level of taurine was higher in transgenic mice, compared with wild-type mice. No significant changes were observed in other metabolites, including mIns. In the study of double-transgenic PS2APP mice, the neurochemical profiles from a 10-μl voxel positioned in the frontal cortex were first obtained for 20-month-old PS2APP mice and age-matched controls (C57BL/6J), and then the cohorts of transgenic mice and control animals were followed from the age of 4 to 24 months with an assessment every 4 months (10). Age-dependent declines of brain NAA and Glu levels were observed that correlated with increasing brain amyloidosis. There was no observed increase of mIns or any other indicator of gliosis with age.

The present study was designed to characterize the neurochemical profile in APP-PS1 AD mice, compared with that of wild-type mice, and to determine the changes in the neurochemical profile with age by using high-resolution, single-voxel ^{1}H MRS. Experiments were conducted to determine specifically whether the ^{1}H MRS changes seen in human AD could be

Abbreviations: ^{1}H MRS, proton magnetic resonance spectroscopy; NAA, *N*-acetylaspartate; Glu, glutamate; mIns, *myo*-inositol; AD, Alzheimer's disease; APP, amyloid-β precursor protein; PS1, presenilin 1; PS2, presenilin 2; tCr, total creatine.

†To whom correspondence should be addressed. E-mail: gosia@cmrr.umn.edu.

www.pnas.org/cgi/doi/10.1073/pnas.0505513102

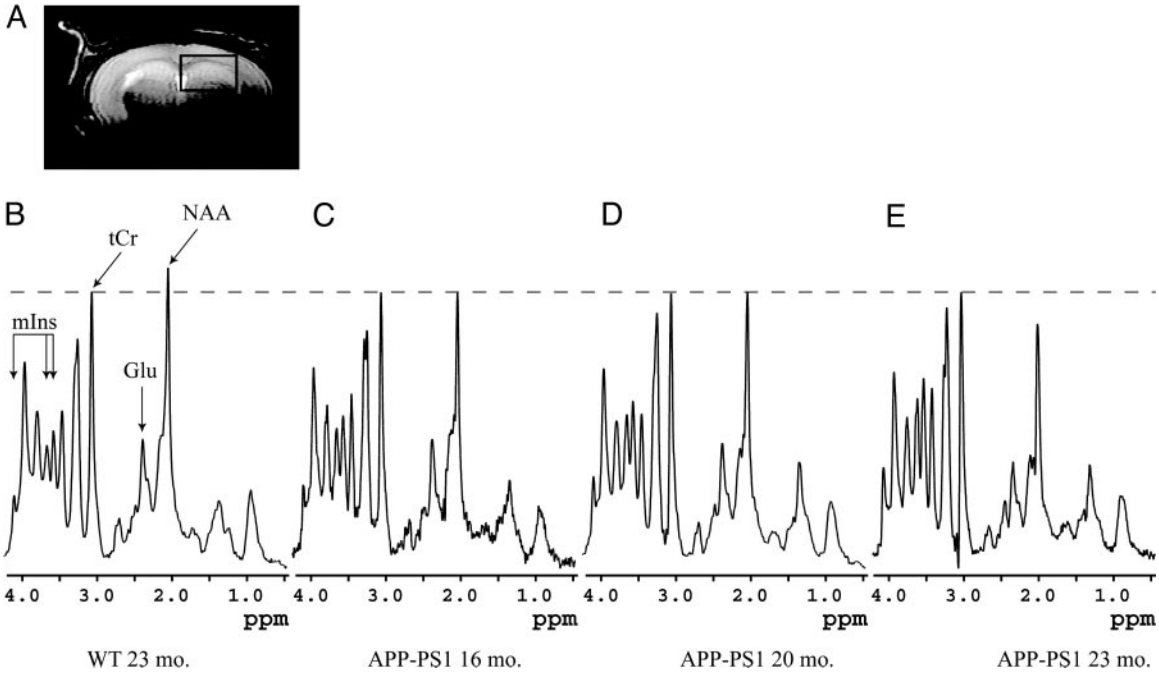

Fig. 1. Representative image and spectra of mouse brain. (*A*) An image of mouse brain with placement and size of the voxel. (*B–E*) Localized *in vivo* ^{1}H MR spectra obtained from 18-μl voxel (box in *A*) from the brain of 23-month-old B6/SJL wild-type (WT) mouse (*B*) and an APP-PS1 mouse scanned at 16 (*C*), 20 (*D*), and 23 (*E*) months of age. The spectra are shown with similar linewidths and with amplitude adjusted by using the total creatine (tCr) peak at 3.03 ppm.

detected in APP-PS1 mice and whether these changes increased with age and hence disease severity.

Materials and Methods

Animals. The double-transgenic mice were cross-bred in-house. Hemizygous transgenic mice (mouse strain: C57B6/SJL; ID no. Tg2576) expressing mutant human APP_{695} containing a double mutation (K670N, M671L) (2) were mated with a strain of homozygous transgenic mice (mouse strain, Swiss Webster/B6D2; ID no. M146L6.2) expressing mutant human PS1 containing a single mutation (M146L) (6).

Animal Preparation. Twenty-seven APP-PS1 (15 males and 12 females) mice and 30 female B6/SJL wild-type mice spanning in age from 66 to 904 days were used in this study. Some of the mice were scanned repeatedly. Eight mice were scanned twice, and two were scanned three times. Additionally, three 624-day-old APP mice were scanned. Mice were anesthetized by using 1.0–1.5% isoflurane and O_2/NO_2 and positioned in a custom-built device to immobilize the head during experiments. Body temperature was maintained at 37°C by warm water circulation, and physiological monitoring was used for temperature, respiration, and ECG as discussed by Jack *et al.* (11). Experimental protocols were approved by the Institutional Animal Care and Use Committees of both the University of Minnesota and the Mayo Clinic in accordance with the National Institutes of Health *Guide for the Care and Use of Laboratory Animals*.

Spectroscopy. *In vivo* ^{1}H spectra were acquired on a 9.4-T, 31-cm horizontal bore magnet (Magnex Scientific, Oxford, U.K.) interfaced with a Varian INOVA console. The magnet was equipped with a gradient insert capable of reaching 300 mT/m in 500 μs (Magnex Scientific). A quadrature 400-MHz ^{1}H surface radiofrequency coil (two loops, 10-mm diameter) was used to transmit and receive. Localizer T_2-weighted multislice rapid acquisition with relaxation enhancement (RARE) images (12) [repetition time (T_R) = 4 s, echo time (T_E) = 60 ms, echo train length = 8, matrix = 256 × 128, slice thickness = 1 mm, 11 slices] were acquired to select an 18-μl volume of interest (voxel) placed in the cortex and hippocampus (Fig. 1*A*). In APP mice, a second voxel (13-μl volume) was centered over the cingulate cortex and extended to include the sensorimotor cortex as described by Dedeoglu *et al.* in ref. 9. Linewidths around 20 Hz for water were obtained after adjusting the first- and second-order shims by using FAST(EST)MAP (13, 14). Spectra were acquired with localization by adiabatic selective refocusing (LASER) (15). After water suppression performed with variable pulse power and optimized relaxation delays (VAPOR) (16), all resonances were excited by using a nonselective numerically optimized adiabatic half-passage pulse (17). Three-dimensional localization was then performed with a pair of adiabatic full-passage pulses in each dimension. The adiabatic half-passage pulse duration was 4 ms, and each adiabatic full-passage pulse was an offset-independent adiabatic pulse, HS1, with a pulse length T_p of 1.5 ms and a bandwidth of 16.7 kHz (15, 18). The echo time was 28 ms, and the repetition time was 3 s. Each free induction decay was acquired with 4,096 complex points and a spectral width of 10 kHz. Free induction decays were stored separately in the memory, and both frequency and phase were corrected based on the total creatine (tCr = creatine and phosphocreatine) signal at 3.03 ppm before summation. Small residual eddy current effects were corrected by using a reference water signal. The spectra used in fitting were a sum of 192 scans obtained in 10 min.

Quantification. The acquired spectra were analyzed by using LCModel 5.2–3 (19, 20) (Stephen Provencher, Oakville, ON, Canada), which calculated the best fit of the experimental spectrum as a linear combination of model spectra. The basis set for LCModel was generated by using MATLAB software (MathWorks, Natick, MA) by simulating the spectral pattern of each metabolite based on the known chemical shifts and *J* couplings (21). In addition, a small signal was added at 0 ppm in all basis spectra for automatic frequency referencing. The experimentally

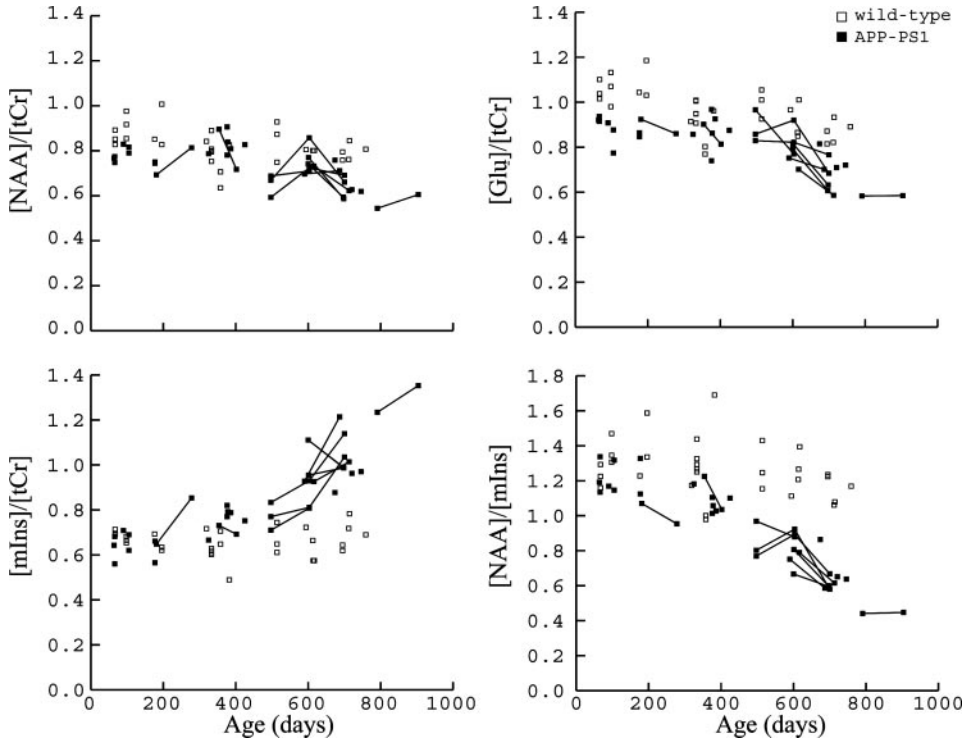

Fig. 2. The ratios of concentration of NAA, Glu, and mIns to tCr and NAA to mIns vs. age of the mice for B6/SJL wild-type (□) and APP-PS1 (■) mice. The connected points refer to the mice that were scanned repeatedly (eight mice were scanned twice, and two mice were scanned three times).

observed spectrum of macromolecules (22) and the simulated spectra of the following 18 metabolites were included in the basis set for LCModel: alanine (Ala), aspartate (Asp), creatine (Cr), γ-aminobutyric acid (GABA), glucose (Glc), Glu, glutamine (Gln), glutathione (GSH), glycerophosphocholine (GPC), phosphocholine (PCho), mIns, lactate (Lac), NAA, N-acetylaspartylglutamate (NAAG), phosphocreatine (PCr), phosphoethanolamine (PE), *scyllo*-inositol (sIns), and taurine. Quantification was obtained by using the tCr (assumed to be 8 mM) resonance as an internal standard. The LCModel fitting was performed over the spectral range from 1.0 to 4.4 ppm.

Statistical Analysis. Statistical analysis was conducted by using SAS software for Windows (version 9.1, SAS Institute, Cary, NC). The ratios of concentration of NAA, Glu, and mIns to tCr and NAA to mIns were compared between wild-type and APP-PS1 mice over time by using analysis of variance. Only the first observation in the case of the repeatedly scanned animals was used in the analysis. A Kruskal–Wallis one-way analysis of variance by ranks test (23) was used to compare the median mIns and taurine levels among the wild-type, APP, and APP-PS1 mice. Subsequent Mann–Whitney *U* tests (23) were used to make pairwise comparisons between different mice groups.

Results

In Fig. 1*A*, a box on an image of a mouse brain shows the position and size of the localized volume (18 μl) from which all spectra were obtained. This voxel was placed over the cortex and the hippocampus. The spectra shown in Fig. 1 *B–E* are representative of the quality consistently achieved in this study. The strong variation in the signal-to-noise ratio in these four spectra comes from the different line-broadening that was applied to make sure that the width of tCr peak is the same in each spectrum. These spectra were analyzed with LCModel to obtain ratios of concentrations of the 16 metabolites with respect to tCr. In Fig. 1 *B–E*, the spectrum obtained from a 23-month-old wild-type mouse is compared with spectra obtained from an APP-PS1 mouse scanned repeatedly at different ages (16, 20, and 23 months old). As the APP-PS1 animal ages, the levels of NAA and Glu decrease, and the level of mIns increases. Even at 16 months, the levels of NAA and Glu are lower than the corresponding levels observed in the wild-type mouse. The level of mIns is higher at 16 months than the corresponding level observed in the wild-type animal.

In Fig. 2, the ratios of the concentrations of certain metabolites obtained with LCModel are plotted vs. the age of the scanned animals (27 APP-PS1 and 30 wild-type mice).

The data from all animals shows a significant decrease in the ratios of concentration of NAA and Glu to tCr [$F(1,56) = 14.89$, $P = 0.0003$; $F(1,56) = 34.75$, $P < 0.0001$, respectively] for wild-type and APP-PS1 mice with increasing age. In addition, the ratios of both NAA and Glu to tCr are lower in APP-PS1 than wild-type mice [$F(1,56) = 11.84$, $P = 0.0011$; $F(1,56) = 33.57$, $P < 0.0001$, respectively]. For the ratio of mIns to tCr, an interaction between age and mouse type is detected [$F(1,55) = 48.75$, $P < 0.0001$], such that an increase in concentration with age in APP-PS1 mice is observed, whereas for wild-type mice no change in the concentration of mIns with age is observed. The estimated ratio of concentration at day 400 is 0.799 [95% confidence interval = (0.770, 0.827)] for APP-PS1 mice and 0.648 [95% confidence interval = (0.621, 0.674)] for wild-type mice. For the ratio of NAA to mIns, an interaction between age and mouse type is detected [$F(1,55) = 26.11$, $P < 0.0001$], such that the concentration decreases with age in transgenic mice, whereas for wild-type mice, no change in concentration with age is observed. This increase in mIns in APP-PS1 mice occurred after about 400 days of age, when amyloid plaque burden is about 4% (total plaque area to cortex surface area in thioflavin S-stained 30-μm histological sections) (7).

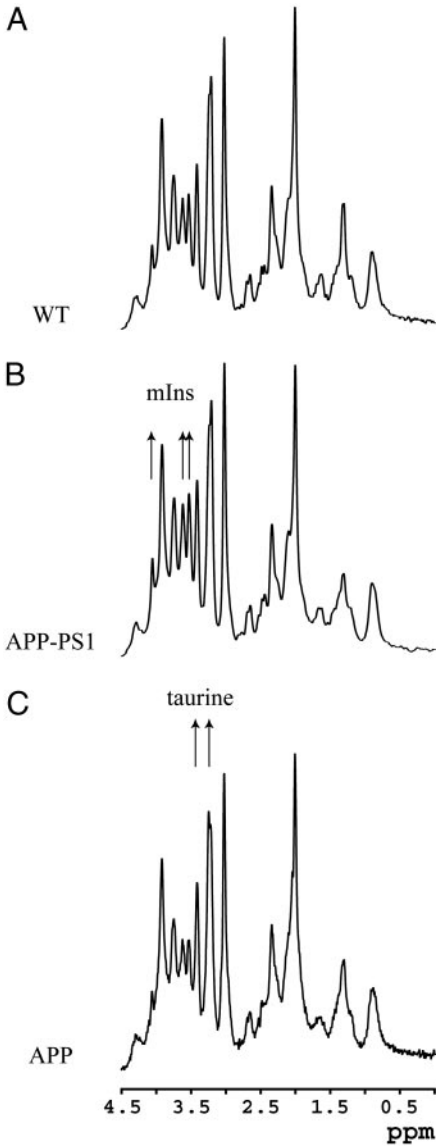

Fig. 3. Localized *in vivo* ^{1}H MR spectra obtained from 18-μl voxel from the brain of age-matched (20 months) B6/SJL wild-type (*A*), APP-PS1 (*B*), and APP (*C*) mice. The spectra are shown with similar linewidths and with amplitude adjusted by using the tCr peak at 3.03 ppm.

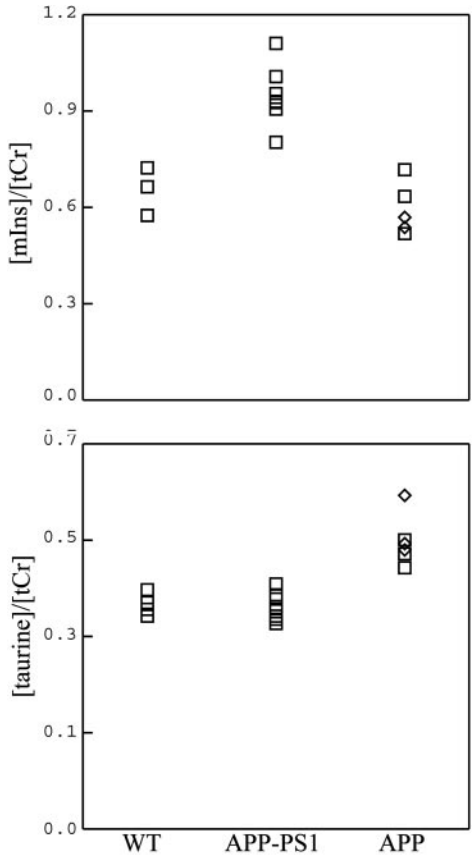

Fig. 4. The ratios of concentration of mIns and taurine to tCr for age-matched (20 months) B6/SJL wild-type (n = 4), APP-PS1 (n = 7), and APP (n = 3) mice. For APP mice, the concentrations are reported for two voxels, and ◇ shows the concentrations obtained from the same voxel that was used in ref. 9.

Changes in the concentration of mIns were not observed in previous studies of mouse AD models (9, 10). In an earlier study performed on 19-month-old APP mice, it was reported that the concentration of taurine rather than mIns is elevated, compared with wild-type animals (9). To further compare the previous study with the current study, three APP mice were examined to compare spectra obtained in the APP-PS1 animals used in the current study with the APP spectra reported in the earlier study (9). Fig. 3 compares spectra obtained from wild-type, APP-PS1, and APP age-matched mice. The observed spectra show clearly that for APP-PS1 mice, the level of mIns is elevated, compared with that of wild-type mice, and that for APP mice, the level of taurine is elevated. Fig. 4 shows the data from age-matched animals of 20 months (four wild-type, seven APP-PS1, and three APP mice). For the APP mice, spectra from an additional voxel placed as close as possible to the cingulate voxel previously used by Dedeoglu *et al.* (9) were obtained (diamonds in Fig. 4). Levels of mIns are significantly higher for APP-PS1, compared with wild-type (Mann–Whitney P = 0.006) and APP mice (Mann–Whitney P = 0.017) but do not differ between wild-type and APP mice (Mann–Whitney P = 0.86). The taurine levels are significantly higher for APP than for APP-PS1 mice (Mann–Whitney P = 0.017) but do not differ between APP and wild-type mice (Mann–Whitney P = 0.057). The taurine levels found in the APP-PS1 mice do not differ from those found in the wild-type mice (Mann-Whitney P = 0.93). Also, the measured levels of mIns and taurine for APP mice from each voxel are similar. This observation suggests that the difference in observed metabolites does not arise from variation in the region of the brain sampled but rather from intrinsic difference between mouse models or possibly from differences in amyloid plaque burden in the 20-month-old APP mice, compared with the APP-PS1 mice used in the present study.

Discussion

A reduction in the levels of NAA and Glu, compared with tCr, with advancing age was found in APP-PS1 mice. Similar findings were observed in APP (9), PS2APP, and wild-type mice (10). The reduction of NAA has been widely used as an indicator of brain pathology and of disease progression in AD patients (24–28). There is, therefore, concordance in the NAA and Glu spectroscopy findings between human AD subjects and all three transgenic mouse models of the disease.

The most striking finding in the present study, however, was a dramatic increase in the concentration of mIns with age in APP-PS1 mice. This observation is very different from those made in studies of APP and PS2APP mice. In the case of APP

mice, the level of taurine rather than mIns increases, and it has been suggested that, in rodents, taurine rather than mIns plays the role of osmoregulator (9). In the present study, the neurochemical profiles obtained for 624-day-old (≈20 months) APP mice from voxels placed in two different locations (where one of the locations mimics the location used in previous study) support the observations published in ref. 9. Two independent studies have shown that, in the APP model, taurine levels increase and mIns levels do not change. In the case of PS2APP mice, no increase in mIns or any other indicator of gliosis was observed, although no mice older than 24 months were examined in that study (10). The authors of that study concluded that the subtle differences between groups may be hidden by the 20% coefficient of variance. In the case of APP-PS1 mice examined in the present study, the most profound increase in mIns level was observed after the age of 600 days (20 months). This increase is attributed to microglial activation in these mice, which may accelerate at around 20 months. Presently available evidence would indicate that the APP-PS1 mouse model most closely matches the complete neurochemical profile exhibited in human AD. It is possible, however, that the elevation of mIns is a function of plaque load rather than the influence of a specific genotype, i.e., the PS1 mutation. APP-PS1 mice develop plaques at a faster rate than APP mice, and therefore at a given age, the plaque load in a cohort of APP-PS1 mice will exceed that in a cohort of APP mice. It remains to be seen whether APP mice with the same plaque load found in 20-month-old APP-PS1 mice also exhibit an elevation in mIns. Further experiments need to be performed to determine whether plaque load or genotype result in mIns elevation. Elevated mIns levels have been found in other animal models of disease, which are characterized by excessive brain gliosis. For example, a 67% increase in the mIns level was reported in hamsters with Creutzfeldt–Jakob disease (29). As in APP-PS1 mice, that increase occurred very late in the clinical phase of the disease, a time that corresponds with the most marked astrocytic reaction (29).

Several useful applications of MRS can be envisioned in AD. Although the experiments were conducted in animals, the age-dependent neurochemical changes observed in APP-PS1 mice are in agreement with previous *in vivo* human MRS studies (24, 26, 27, 30). Depressed NAA and Glu and elevated mIns have been used for diagnostic purposes clinically (28), whereas longitudinal measures can be used to assess disease progression in humans (31, 32). Activated microglia accumulate at the periphery of amyloid plaques both in human AD and in transgenic APP-PS1 mice. Some believe that the microglial activation may be responsible for at least some of the neuronal damage that characterizes AD. The most striking finding was the age-dependent elevation of mIns in the APP-PS1 mice, but depression of Glu and NAA also was present. Data in Fig. 2 illustrate the complementary nature of information obtained from NAA (or Glu) and mIns. Wild-type and APP-PS1 mice were completely differentiated at ages >12 months by forming the ratio of NAA/mIns. Measures of this ratio could therefore serve as a highly sensitive *in vivo* surrogate indicator of therapeutic efficacy in trials of agents designed to reduce neurotoxicity mediated by microglial activation. Drug investigational studies with ^{1}H MRS in APP-PS1 mice appear particularly attractive, because these mice exhibit an ^{1}H MRS profile analogous to that present in human AD subjects. Because of its noninvasive and repeatable nature, MRS in transgenic models of AD could substantially accelerate drug discovery for this condition.

We thank Dr. Karen Duff (Nathan Kline Institute, Orangeburg, NY) for the PS1 transgenic mouse line, Dawn M. Gregor for mouse breeding and genotyping, and Dr. Jamie D. Walls for comments about the paper. This work was supported by National Institutes of Health Grants RR08079, AG22034, and CA92004; the W. M. Keck Foundation; the Mind Institute; and the Minnesota Partnership for Biotechnology and Medical Genomics.

1. Games, D., Adams, D., Alessandrini, R., Barbour, R., Berthelette, P., Blackwell, C., Carr, T., Clemens, J., Donaldson, T., Gillespie, F., *et al.* (1995) *Nature* **373,** 523–527.
2. Hsiao, K., Chapman, P., Nilsen, S., Eckman, C., Harigaya, Y., Younkin, S., Yang, F. & Cole, G. (1996) *Science* **274,** 99–102.
3. Sturchler-Pierrat, C., Abramowski, D., Duke, M., Wiederhold, K. H., Mistl, C., Rothacher, S., Ledermann, B., Burki, K., Frey, P., Paganetti, P. A., *et al.* (1997) *Proc. Natl. Acad. Sci. USA* **94,** 13287–13292.
4. Chishti, M. A., Yang, D. S., Janus, C., Phinney, A. L., Horne, P., Pearson, J., Strome, R., Zuker, N., Loukides, J., French, J., *et al.* (2001) *J. Biol. Chem.* **276,** 21562–21570.
5. Duff, K., Eckman, C., Zehr, C., Yu, X., Prada, C. M., Perez-Tur, J., Hutton, M., Buee, L., Harigaya, Y., Yager, D., *et al.* (1996) *Nature* **383,** 710–713.
6. Holcomb, L., Gordon, M. N., McGowan, E., Yu, X., Benkovic, S., Jantzen, P., Wright, K., Saad, I., Mueller, R., Morgan, D., *et al.* (1998) *Nat. Med.* **4,** 97–100.
7. Wengenack, T. M., Whelan, S., Curran, G. L., Duff, K. E. & Poduslo, J. F. (2000) *Neuroscience* **101,** 939–944.
8. Richards, J. G., Higgins, G. A., Ouagazzal, A. M., Ozmen, L., Kew, J. N., Bohrmann, B., Malherbe, P., Brockhaus, M., Loetscher, H., Czech, C., *et al.* (2003) *J. Neurosci.* **23,** 8989–9003.
9. Dedeoglu, A., Choi, J. K., Cormier, K., Kowall, N. W. & Jenkins, B. G. (2004) *Brain Res.* **1012,** 60–65.
10. von Kienlin, M., Kunnecke, B., Metzger, F., Steiner, G., Richards, J. G., Ozmen, L., Jacobsen, H. & Loetscher, H. (2005) *Neurobiol. Dis.* **18,** 32–39.
11. Jack, C. R., Jr., Garwood, M., Wengenack, T. M., Borowski, B., Curran, G. L., Lin, J., Adriany, G., Grohn, O. H., Grimm, R. & Poduslo, J. F. (2004) *Magn. Reson. Med.* **52,** 1263–1271.
12. Hennig, J., Nauerth, A. & Friedburg, H. (1986) *Magn. Reson. Med.* **3,** 823–833.
13. Gruetter, R. (1993) *Magn. Reson. Med.* **29,** 804–811.
14. Gruetter, R. & Tkáè, I. (2000) *Magn. Reson. Med.* **43,** 319–323.
15. Garwood, M. & DelaBarre, L. (2001) *J. Magn. Reson.* **153,** 155–177.
16. Tkac, I., Starcuk, Z., Choi, I. Y. & Gruetter, R. (1999) *Magn. Reson. Med.* **41,** 649–656.
17. Garwood, M. & Ke, Y. (1991) *J. Magn. Reson.* **94,** 511–525.
18. Silver, M. S., Joseph, R. I. & Hoult, D. I. (1984) *J. Magn. Reson.* **59,** 347–351.
19. Provencher, S. W. (1993) *Magn. Reson. Med.* **30,** 672–679.
20. Provencher, S. W. (2001) *NMR Biomed.* **14,** 260–264.
21. Govindaraju, V., Young, K. & Maudsley, A. A. (2000) *NMR Biomed.* **13,** 129–153.
22. Pfeuffer, J., Tkac, I., Provencher, S. W. & Gruetter, R. (1999) *J. Magn. Reson.* **141,** 104–120.
23. Sheskin, D. (2000) *Handbook of Parametric and Nonparametric Statistical Procedures* (Chapman & Hall/CRC, Boca Raton, FL).
24. Miller, B. L., Moats, R. A., Shonk, T., Ernst, T., Woolley, S. & Ross, B. D. (1993) *Radiology* **187,** 433–437.
25. Moats, R. A., Ernst, T., Shonk, T. K. & Ross, B. D. (1994) *Magn. Reson. Med.* **32,** 110–115.
26. Shonk, T. K., Moats, R. A., Gifford, P., Michaelis, T., Mandigo, J. C., Izumi, J. & Ross, B. D. (1995) *Radiology* **195,** 65–72.
27. Shonk, T. & Ross, B. D. (1995) *Magn. Reson. Med.* **33,** 858–861.
28. Ross, B. D., Bluml, S., Cowan, R., Danielsen, E., Farrow, N. & Tan, J. (1998) *Neuroimag. Clin. N. Am.* **8,** 809–822.
29. Behar, K. L., Boucher, R., Fritch, W. & Manuelidis, L. (1998) *Magn. Reson. Imaging* **16,** 963–968.
30. Kantarci, K., Reynolds, G., Petersen, R. C., Boeve, B. F., Knopman, D. S., Edland, S. D., Smith, G. E., Ivnik, R. J., Tangalos, E. G. & Jack, C. R., Jr. (2003) *Am. J. Neuroradiol.* **24,** 843–849.
31. Adalsteinsson, E., Sullivan, E. V., Kleinhans, N., Spielman, D. M. & Pfefferbaum, A. (2000) *Lancet* **355,** 1696–1697.
32. Jessen, F., Block, W., Traber, F., Keller, E., Flacke, S., Lamerichs, R., Schild, H. H. & Heun, R. (2001) *Neurology* **57,** 930–932.